energies

MDPI

Article

Double Cathode Modification Improves Charge Transport and Stability of Organic Solar Cells

Tao Lin * and Tingting Dai

Department of Physics, Beijing Technology and Business University, Beijing 100048, China
* Correspondence: lintao@btbu.edu.cn

Abstract: Introducing a cathode modification layer is an effective method to obtaining highly efficient organic solar cells (OSCs) and improving their stability. Herein, we innovatively introduced a double cathode modification layer (SnO_2/ZnO) into a non-fullerene OSCs based on PM7:IT-4F and explored the mechanisms. The effects of SnO_2/ZnO film on charge carriers transfer in OSCs are studied via a variety of electrical testing methods including Photo-CELIV measurements. As a result, a cathode buffer layer with low recombination rate and high carrier mobility could be introduced, which is beneficial to electron transport and collection. The champion device based on the double cathode modification layer acquires an efficiency of 12.91%, obviously higher than that of the single cathode modification layer (SnO_2 or ZnO) device. Moreover, The SnO_2/ZnO double layer is demonstrated to be of great help in the improvement of device stability, and our work could provide a new inspiration for the preparation of OSCs cathode modification layer.

Keywords: organic solar cells; double cathode modification layer; charge transport

check for updates

Citation: Lin, T.; Dai, T. Double Cathode Modification Improves Charge Transport and Stability of Organic Solar Cells. *Energies* **2022**, *15*, 7643. https://doi.org/10.3390/en15207643

Academic Editor: Fujun Zhang

Received: 4 October 2022
Accepted: 13 October 2022
Published: 16 October 2022

1. Introduction

Over recent years, remarkable progress have been made in the field of organic solar cells (OSCs), which is considered a potential candidate to accessing clean energy [1–3]. Most of these breakthroughs are owing to synthetic new materials [4–7], optimization of device structure [8–10], morphology control of active layers [11–13], as well as adopting the interface modification layers which have been considered an efficient method to achieve high-efficient and stable OSCs for the advantages of adjusting the energy barrier between electrode and organic active layers and improving the charge extraction ability of the electrode [14–16]. Poly(3,4-(ethylenedioxy)thiophene):poly(styrenesulfonate) (PEDOT:PSS) is the most commonly used anode buffer layer materials in the normal OSCs fabrication for their superior hole transport capability, good transparency in the spectral response range and so on [17,18]. While for cathode buffer layer, the most commonly used modification materials can be divided into two categories: inorganic materials and organic materials. Inorganic materials are mainly metal oxides, such as zinc oxide (ZnO) [19,20], titanium oxide (TiO_X) [21], lithium fluoride (LiF) [22]. For organic materials, poly[(9,9-bis(3′-(N,N-dimethylamino)propyl)-2,7-fluorene)-alt-2,7-(9,9 –dioctylfluorene)] (PFN) [23–25], Polyethylenimine ethoxylated (PEIE) [26], perylene diimide derivatives (PDIN-o) [27,28] and PDIN [29,30] are usually used.

Except the power conversion efficiency (PCE), the long-term stability still remains to be a great challenge of OSCs development which is always overlooked by high-efficiency device reports. At present, the main way to enhance the lifetime of OSCs is to consider how to slow down the rate of erosion caused by moisture and oxygen. Methods have been taken, such as synthesizing hydrophobic organic materials, encapsulating devices, and so on [31–33]. Moreover, regulation of electrode modification layer has been considered an important approach to resist moisture and oxygen molecules into device [34,35], which can affect both active layer and electrode for the special location in the device structure.

Therefore, the study of electrode modification layer is of great significance for enhancing device efficiency and stability simultaneously.

In this work, we fabricated the inverted OSCs based on Poly[(2,6-(4,8-bis(5-(2-ethylhexyl-3-chloro)thiophen-2-yl)-benzo[1,2-b:4,5-b′]dithiophene))-alt-(5,5-(1′,3′-di-2-thienyl-5′,7′-bis(2-ethylhexyl)benzo[1′,2′-c:4′,5′-c′]dithiophene-4,8-dione)] (PM7) as donor and 3,9-bis(2-methylene-((3-(1,1-dicyanomethylene)-6,7-difluoro)-indanone))-5,5,11,11-tetrakis(4-hexylphenyl)-dithieno[2,3-d:2′,3′-d′]-s-indaceno[1,2-b:5,6-b′]dithiophene (IT-4F) as acceptor with SnO_2/ZnO (ZnO and SnO_2 for comparison) as cathode modification layer. It should be noted that the use of a double layer of inorganic material as a charge transport layer (electrode modification layer) has been previously used in devices based on other material systems (such as perovskite) [36–38], but to our knowledge has not been used in PM7:IT-4F based OSCs. SnO_2/ZnO film improves the power conversion efficiency (PCE) of the device to 12.91% with FF of 70%, J_{SC} of 20.04 mA/cm^2 and V_{OC} of 0.92 V, due to the improvement of charge transfer/collection. Moreover, compared with the single cathode modification layer (ZnO, SnO_2), the adoption of SnO_2/ZnO film effectively improves the stability of the device, with a reduced rate of dark-degradation in both air and nitrogen. Taken together, this work would provide insights into OSCs interfacial modification mechanism study with new revelation in-depth elucidation of the underlying mechanisms associated with improved device efficiency and stability, which will provide insights into OSCs interfacial modification studies.

2. Materials and Methods

The active polymer PM7 and Non-fullerene small molecule material IT-4F were used as donor and acceptor, respectively. Active layer solvent is o-Xylene (OX). ZnO, SnO_2 and MoO_3 were utilized in the preparation of electron-transport layer and anode buffer layer, respectively. Among them, ZnO was prepared by sol gel with $Zn(Ac)_2{\cdot}2H_2O$, C_2H_7NO and $C_3H_8O_2$. PM7 and small molecule acceptor material IT-4F were purchased from 1-Material Inc (Dorval, Quebec, Canada). Organic reagents such as OX, DClO, C_2H_7NO, $C_3H_8O_2$ and CH_2Cl_2 were acquired from Sigma-Aldrich (Merck KGaA, Darmstadt, Germany). $Zn(Ac)_2{\cdot}2H_2O$ and SnO_2 were purchased from J&K Scientific (Beijing, China). All the materials were used as received without any further treatment. Donor material PM7 and acceptor material IT-4F were put into a solution bottle (Agilent, Santa Clara, California, United States) in a mass ratio of 1.25:1, and added CH_2Cl_2 (1.5 µL/mg). Then left the bottle in glove box (Mikrouna, Shanghai, China) with high purity nitrogen to dry thoroughly and await further processing. Once the organic materials (PM7 and IT-4F) dried, donor and acceptor materials were dissolved in OX (20 mg/mL) by heating 60 °C with stirring for 6 h. As for ZnO precursor solution, in briefly, 164.61 mg of $Zn(Ac)_2{\cdot}2H_2O$ and 45.81 mg of C_2H_7NO (molar ratio 1:1) were dissolved in 1 mL $C_3H_8O_2$ and then stirred continuously in the dark, heating 60 °C, until the solids completely dissolved (almost 12 h). SnO_2 solution (purchased from J&K Scientific, Beijing, China) was diluted by adding deionized water in a volume ratio of 1:6 for further use.

Devices were fabricated by featuring three kinds of cathode modification layer (ZnO, SnO_2 and SnO_2/ZnO), respectively, in an inverted structure: indium tin oxide (ITO)/buffer layer/PM7:IT-4F/MoO_3/Ag (Figure 1a). The chemical structural formulas of the donor material PM7 and the acceptor material IT-4F used in the experiment are shown in Figure 1b, c. For the device preparation, all the devices were fabricated on cleaned ITO-coated glass substrates (sheet resistance: 15 Ω/Sq), cleaned by followed steps with sequential sonication in deionized water, acetone, ethanol each for 20 min. Wait until the ITO-coated substrate fully dries by high purity nitrogen for further ultraviolet-ozone treatment for 8 min. The buffer layer was spin coated on the treated ITO substrates as cathode modification layer using a sol-gel process. Next, it was thermal-annealed at 150 °C for 30 min (for ZnO), 200 °C for 60 min (for SnO_2) and 180 °C for 40 min (for SnO_2/ZnO). Subsequently, place the prepared ITO/cathode modification layer films into the glove box filled with high purity nitrogen (O_2 and H_2O content < 0.01 ppm), and then a blend layer of PM7:IT-4F was

spin-coated on the films and dried for 30 min to obtain the dry active layer film. Place the ITO/cathode modification layer/active layer in a thermal evaporative coating instrument (Mikrouna, Shanghai, China), vacuumed to a vacuum of 1.5×10^{-6} Torr, and then MoO_3 and silver were successively deposited as anode buffer layer and anode, respectively.

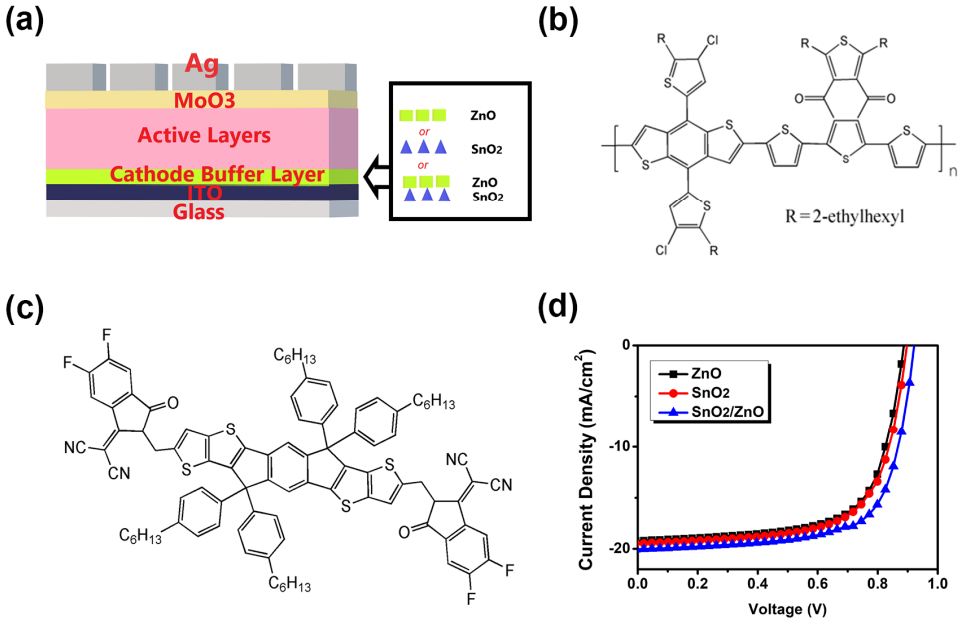

Figure 1. (**a**) Device architecture and photoactive materials; (**b**) PM7 (where n indicates the degree of polymerization); (**c**) IT-4F; (**d**) The J-V characteristic curves of the OSCs with ZnO, SnO_2 and SnO_2/ZnO cathode buffer layers.

The thickness for each layer of the device (including anode modification layer, cathode modification layer, active layer and Ag electrode) was measured via the Dektak XT Stylus Profile (Bruker Corporation, Billerica, MA, USA). The UV-vis absorption spectra of PM7:IT-4F films (with different electronic transport layer, including ZnO, SnO_2 and SnO_2/ZnO) were recorded using a U3900H spectrophotometer (Hitachi, Tokyo, Japan). The Keithley 2400 measurement unit (Tektronix Inc., Beaverton, OR, United States) was used to obtain the current density-voltage (J-V) characteristic curves (AM 1.5G) of each device (San-Ei Electric, Osaka, Japan). The EQE curves of each device was measured by a SC100 solar cell QE/IPCE testing system (Zolix Instruments CO., Ltd., Beijing, China). In addition, The Paios carrier characterization system (FLUXiM AG, Winterthur, Switzerland) was utilized to measure the TPV/TPC and Photo-CELIV.

3. Results and Discussion

3.1. Device Performance

As shown in, organic solar cells were fabricated with different electron transport layer (ZnO, SnO_2 and SnO_2/ZnO). The J-V curves of the devices are shown in Figure 1d, while the relevant photovoltaic parameters are listed in Table 1, including short-circuit current density (J_{SC}), open-circuit voltage (V_{OC}), fill factor (FF) and power conversion efficiency (PCE). Meanwhile, the parameters of OSCs based on PM7:IT-4F active layer in other studies are presented in Table 2 for reference. By modified with SnO_2/ZnO, the device exhibits a PCE of 12.9% with a J_{SC} of 20.04 mA/cm^2, a V_{OC} of 0.91 V and a FF of 70%. For comparation, the device with single cathode buffer layer ZnO shows a PCE of 11.45%, and J_{SC}, V_{OC} and FF are 19.22 mA/cm^2, 0.88 V and 67%, respectively. While the SnO_2 modified device shows a PCE of 12.03%, a J_{SC} of 19.45 mA/cm^2, a V_{OC} of 0.90 V and a FF of 68%.

Table 1. Photovoltaic performance of devices with ZnO, SnO_2 and SnO_2/ZnO films.

	J_{sc} (mA/cm^2)	V_{oc} (V)	FF	PCE (%)
ZnO	19.22 [a] (19.06 [b] ± 0.15)	0.88 [a] (0.88 [b] ± 0.01)	0.67 [a] (0.66 [b] ± 0.01)	11.45 [a] (11.42 [b] ± 0.04)
SnO_2	19.45 [a] (19.28 [b] ± 0.12)	0.90 [a] (0.90 [b] ± 0.01)	0.68 [a] (0.68 [b] ± 0.01)	12.03 [a] (11.92 [b] ± 0.12)
SnO_2/ZnO	20.04 [a] (19.72 [b] ± 0.29)	0.92 [a] (0.91 [b] ± 0.01)	0.70 [a] (0.69 [b] ± 0.01)	12.91 [a] (12.66 [b] ± 0.24)

[a] For champion device. [b] For average of 30 devices.

Table 2. Photovoltaic parameters of devices in relevant research.

Device Structure	J_{sc} (mA/cm^2)	V_{oc} (V)	FF	PCE (%)
ITO/NP-ZnO/PM7:IT-4F/MoO_3/Al [39]	20.9	0.88	0.71	13.1
ITO/PEDOT:PSS/PM7:IT-4F/PDINO/Al [40]	20.5	0.85	0.77	13.4
ITO/ZnO/PM7:IT-4F/MoO_3/Ag [41]	20.21	0.86	0.72	12.48
ITO/ZnO/PM7:IT-4F/MoO_3/Ag [42]	15.8	0.90	0.64	9.1
ITO/PEDOT:PSS/PM7:IT-4F/PFN-Br/Al [43]	17.14	0.93	0.73	11.72
ITO/PEDOT:PSS/PM7:IT-4F/PFN-Br/Al [44]	20.48	0.87	0.55	9.77
ITO/ZnO/PM7:IT-4F/MoO_3/Ag [45]	20.47	0.90	0.69	12.74
This work	20.04	0.92	0.70	12.91

Compared to the device with the ZnO buffer layer the SnO_2 cathode modifier layer device shows a significant improvement of FF and J_{SC}, which is due to the fact that SnO_2 film is smoother than ZnO film (see Figure S1) and would form better contact with the active layer. While the device base on SnO_2/ZnO modification layer gives the best performance for all parameters, we think there are two main reasons for this. On one hand, it has been shown that preparing SnO_2 on ITO can improve the surface of ITO [46], and we speculate that inserting a layer of SnO_2 between ITO and ZnO could improve the quality of ZnO film, which is more conducive to the transmission of electrons between the active layer and the cathode electrode by reducing the generation of traps at the interface and the recombination of charge at the cathode electrode. On the other hand, the surface of SnO_2 film usually shows a large number of defects, mainly oxygen vacancies (donor defects) [47,48], cover the ZnO film on the SnO_2 cathode buffer layer may passivate these surface defects, which can reduce the possible leakage current between the active layer and the electrode, provide an effective transfer channel for the transmission of electrons from the active layer to the cathode electrodes, reduce the recombination of carriers, so as to improve the FF and J_{SC} of the device. The improvement of the V_{OC} should be mainly attributed to that the double cathode modification layers optimize the interface layer contact and reduce the energy barrier between the electrode and the active layer. Meanwhile, the calculated work function of ZnO, SnO_2 and SnO_2/ZnO modified electrodes are 4.57, 4.03 and 4.26 eV (see Figure S2 and Table S1), respectively, considering that the LUMO level of the acceptor material IT-4F is −4.15 eV, the energy level between the active layer and the SnO_2/ZnO modified electrode is more compatible, which is more conducive to the transmission of electrons.

3.2. Characterization of Opto-Electronic Properties

The ultraviolet-visible absorption spectrum and external quantum efficiency spectra of the devices with ZnO, SnO_2 and SnO_2/ZnO (Figure 2) were measured to further understand the effect of the double-cathode buffer layer on the improvement of device performance. As the UV-Vis absorption spectrum shown in Figure 2a, there is no significant increase in light absorption for device based on SnO_2/ZnO, indicating that the increase of J_{SC} is not due to the improvement of the absorption of the film. As we all know, the improvement of J_{SC} is associated with the ability to capture photons, the transmission and collection of charges [49]. Therefore, the improvement of J_{SC} by the double cathode modification layer

should be attributed to the improvement of charge transfer/collection in device. The EQE spectrum of devices with different cathode buffer layers were measured (Figure 2b). It can be seen that the curve of the double modification layer device is improved as a whole compared with that of the single modification layer devices, and the J_{SC} calculated via integrating the EQE curves were in good agreement with the J_{SC} obtained from the J-V curves (within 5% mismatch). Considering the results of UV-Vis absorption spectrum, we illustrate that the increase in J_{SC} corresponds to the improvement of the charge transport and the reduce of the charge recombination.

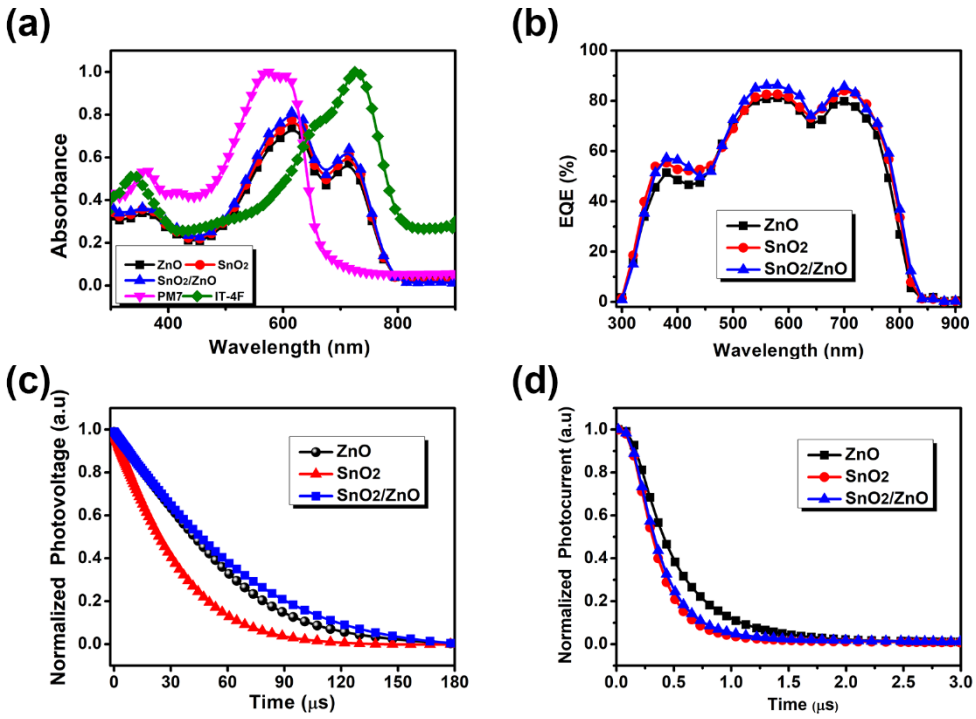

Figure 2. (**a**) UV-Vis absorption spectra and (**b**) the EQE spectra of the devices; Normalized (**c**) TPV and (**d**) TPC decay curves of the device with different cathode buffer layers.

Transient photovoltage (TPV) and transient photocurrent (TPC) measurements were applied to further study the charge transfer and charge extraction dynamics of the devices with different cathode buffer layers (ZnO, SnO_2 and SnO_2/ZnO).

TPV measurement can be utilized to analyze the charge recombination characteristic of the OSCs by exploring the decay lifetime via recording the voltage decay process under open circuit condition [50]. The TPV curve is recorded by keeping the device at open circuit voltage under bias-illumination [51,52]. On this basis, the device is applied an additional LED pulse to generate additional charges, and then the photovoltage decays exponentially. Meanwhile, the charge carrier lifetime can be calculated directly from the decay curve. In TPV analysis, the charge recombination time can be derived from a single exponential equation $V = Aexp(-t/\tau)$ (where A is a constant of the fitted peak height, t is the time and τ is the decay time) [52,53]. By fitting the TPV curves in Figure 2c, the transient photovoltage decay lifetime of ZnO, SnO_2 and SnO_2/ZnO modified devices is 69.18 μs, 34 μs and 77 μs, respectively (Table 3). The results suggest that the SnO_2/ZnO layer is contributing to prolong the transient photovoltage decay lifetime of the OSCs. A short decay lifetime results from a premature recombination of charge carriers, which means the inefficient charge transport and low power conversion efficiency [54]. Compared to the device modified with single cathode buffer layer (ZnO or SnO_2), the device with SnO_2/ZnO have prolonged decay lifetime and exhibited higher device performance, which indicates the reduced charge carrier recombination due to the SnO_2/ZnO modification. For the SnO_2 modified device with the shortest decay lifetime, we speculate that the unfavorable energy

level arrangement at the interface between SnO_2 modified electrode and the active layer leads to charge accumulation and thus increased recombination.

Table 3. The parameters derived from TPV/TPC and Photo-CELIV measurements for the devices with different cathode buffer layers.

	τ_{TPV} (μs)	τ_{TPC} (μs)	Carrier Mobility ($cm^2 \cdot V^{-1} \cdot s^{-1}$)
ZnO	69.18	0.45	8.10×10^{-5}
SnO_2	34.27	0.31	9.89×10^{-5}
SnO_2/ZnO	77.42	0.33	1.54×10^{-4}

TPC measurement is a method applied to obtain the charge extraction time τTPC of the OSCs via exponential fitting the normalized transient photocurrent decay curves derived from recording the current response of an optical step under short-circuit condition [55,56], and the short τTPC stands for good carrier transport and extraction [57]. By fitting the TPC curves in Figure 2d, the charge extraction time of devices modification by difference cathode buffer layer are summarized in Table 3. The charge extraction time for ZnO modification layer device is 0.45 μs, for SnO_2 is 0.31 μs, and for double cathode modification layer device is 0.33 μs. Due to the vertical growth of SnO_2 nanocrystal and the characteristic of hole blocking [58], the τTPC of the device modified with SnO_2 is shorter than other devices. The device modified with ZnO film shows the longest charge extraction time, which could result from the ZnO film fabricated in this study is amorphous, the electron transport characteristic of which is inferior to crystalline ZnO film [59]. However, the device prepared by covering a SnO_2 layer before preparing the ZnO film as cathode modification layer (SnO_2/ZnO) shows a significant reduce in extraction time, compared to the device that directly fabricated ZnO film. The result indicates that the double cathode modification layer effectively enhances the efficiency of OSCs via improving charge collection at the electrode.

Through analyzing the characterization of carrier lifetime and charge extraction, we can conclude that the significant enhancement caused by double cathode modification layer (SnO_2/ZnO) is mainly based on the improvement of the charge transfer and collection in the device, which is in good agreement with UV-vis and EQE results.

Photo-induced charge extraction linear increasing voltage (Photo-CELIV) measurement is applied to gain the carrier mobility of OSCs modified with ZnO, SnO_2 and SnO_2/ZnO [56,60], which is an effective research technology in revealing the internal charge transport characteristics of the device in operation. The corresponding photocurrent curves recorded by Photo-CELIV measurement are shown in Figure 3. A white LED light pulse is applied to the device tested in Photo-CELIV experiment, and then a linearly boosted signal is used to extract the photo-generated free charger inside the device [56,61]. During the Photo-CELIV test, the recorded photo-generated current curves show a rise, then slowly decrease, and finally tend to equilibrium. The charge carrier mobility can be calculated by the formula $\mu = 2d^2/3At_{max}^2 \cdot 1/(1 + 0.36\Delta j/j_{disp})$ (where μ is the charge carrier mobility, A is the ramp rate, d is the active layer thickness (~120 nm), Δj is the peak current minus the displacement current, $1 + 0.36\Delta j/j_{disp}$ is an empirical correction for electric field redistribution, j_{disp} is the displacement current, t_{max} is the time when the current reaches the peak) [61]. The values of carrier mobility for the devices modified with ZnO, SnO_2 and SnO_2/ZnO are summarized in Table 3 calculated by the above formula. The device modified with these three kinds of buffer layers performed a charge carrier mobility of 8.10×10^{-5} $cm^2 \cdot V^{-1} \cdot s^{-1}$, 9.89×10^{-5} $cm^2 \cdot V^{-1} \cdot s^{-1}$ and 1.54×10^{-4} $cm^2 \cdot V^{-1} \cdot s^{-1}$, respectively, which reveals the improved carrier transport between the two electrodes, is one of the main mechanisms for the improving of device performance.

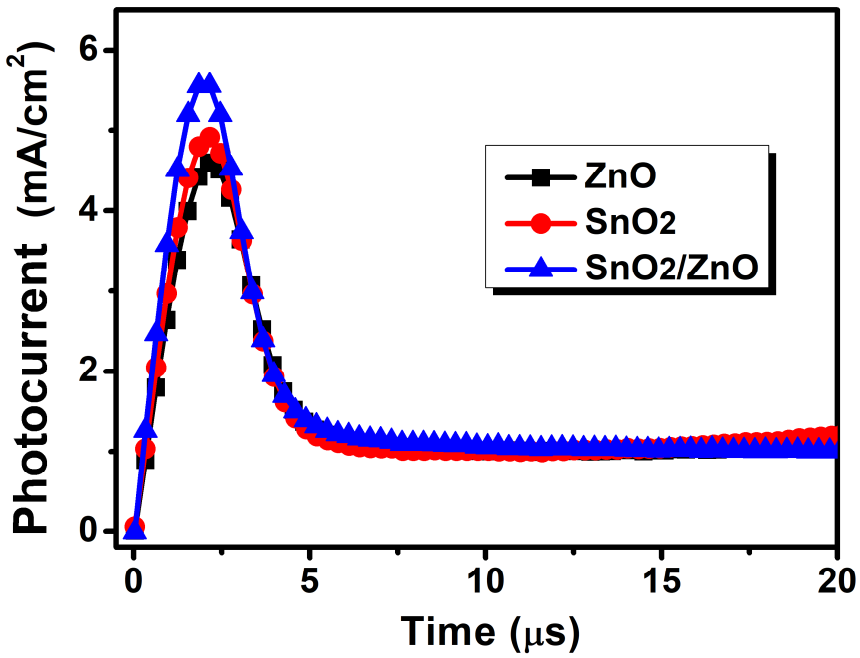

Figure 3. Photo-CELIV curves of the device with different cathode buffer layers.

In order to further investigate the charge transport and carrier recombination properties, the relationship between V_{OC}/J_{SC} and light intensity (P_{light}) of the device was measured (Figure 4).

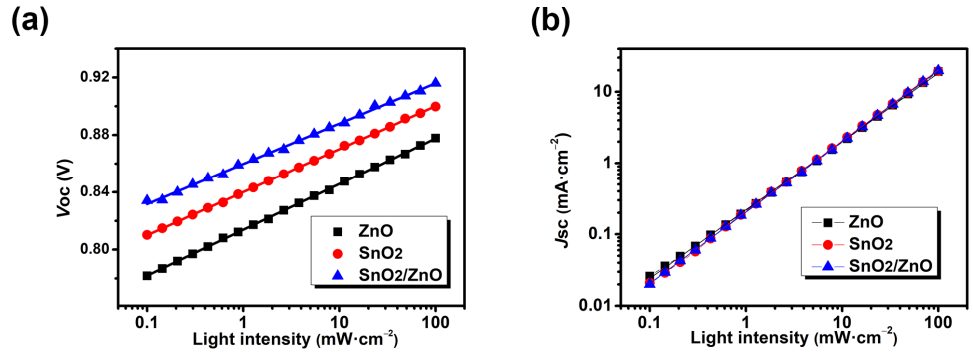

Figure 4. The light intensity dependence of (**a**) V_{OC} and (**b**) J_{SC} of the device with different cathode buffer layers.

The dependence of V_{OC} on P_{light} (see Figure 4a) is consistent with the logarithmic relationship: $V_{OC} \propto \beta \ln P_{light}$, where $\beta = n\kappa T/q$, κ is the Boltzmann constant value, n is the ideal factor, T is the absolute temperature and q is the elementary charge. The ideal factor n is usually between 1 to 2, which means that β is usually between $1\kappa T/q$ to $2\kappa T/q$. The β value symbolizes the competitive relationship between trap-assisted Shockley-Read-Hall (SRH) recombination and bimolecular recombination [57]. In general, the β values tend to $1\kappa T/q$ suggests that bimolecular recombination is the dominant factor, whereas β values tend to $2\kappa T/q$ indicates additional Shockley-Read-Hall (SRH) recombination have involved [62]. The lower β value means the Shockley-Read-Hall (SRH) recombination is the weaker factor in carrier recombination, and the SRH recombination is associated with interface defects that cause electrons and holes to be trapped and then recombined. The fitted lines for the devices modified with ZnO, SnO_2 and SnO_2/ZnO, showed the β values of $1.22\kappa T/q$, $1.16\kappa T/q$ and $1.08\kappa T/q$, respectively (Table 4), indicating that SnO_2/ZnO film contributes to the suppressed SRH recombination with less interface trap and more efficient

charge transfer. Furthermore, the suppressed trap-assisted recombination results in higher FF and V_{OC}, which is in good agreement with the TPV and TPC results.

Table 4. The values of the light intensity dependence of J_{SC} and V_{OC} of the device with different cathode buffer layers.

	α	β (κT/q)
ZnO	0.9594	1.22
SnO_2	0.9977	1.16
SnO_2/ZnO	0.9949	1.08

In addition, the dependence of the J_{SC} value on P_{light} were investigated for each device to further understand the bimolecular recombination and space charge accumulation in different devices. By fitting the lines in Figure 4b, the α values for devices modified with ZnO, SnO_2 and SnO_2/ZnO are 0.9594, 0.9977 and 0.9949, respectively. Following in theoretical consideration, the bimolecular recombination is associated by the α value in a logarithmic plot of $J_{SC} \propto P_{light}{}^{\alpha}$. Compared to the ZnO modified device, the α values of the SnO_2 and SnO_2/ZnO modified devices are more tend to 1 indicating the introduction of SnO_2 could effectively suppress bimolecular recombination in the device. This may be due to the fact that SnO_2 can effectively block holes [58] and improve the quality of ZnO film. Meanwhile, the addition of SnO_2 provides a more efficient charge transfer channel for the transport of electrons, and improves the ability to extract charge at the cathode.

In briefly, SnO_2/ZnO device showed relatively suppressed trap-assisted recombination and bimolecular recombination, which is the main reason for improvement of OSC performance, and in line with the TPV/TPC and UV-Vis results.

3.3. Improving Device Stability via SnO_2/ZnO

There has been a lack of reports on the long-term stability of high-efficiency non-fullerene OSCs. Here we specifically tested and compared the long-term stability of devices based on three cathode modification layers. Figures 5 and 6 show the dark-degradation curves of the photovoltaic characteristic parameters of the OSCs in nitrogen atmosphere and air conditions. As shown in Figure 5, the values of efficiency after six months for ZnO, SnO_2 and (SnO_2/ZnO) modified devices are decay to 80%, 87% and 93% of the initial device, respectively. The results suggest that the device modified with SnO_2/ZnO film is able to avoid the direct contact between ITO and ZnO film effectively. Meanwhile, cover the SnO_2 layer with a ZnO film can passivate the surface defects of SnO_2 film and prevent downward penetration of molecules from the active layer into the electrode. In briefly, the improvement of stability for the OSCs from the introduction of SnO_2/ZnO film as cathode modification layer results in the life extension of OSCs in nitrogen atmosphere.

To confirm the environmental stability of SnO_2/ZnO modified device, we evaluated the stability for each device modified with single and double modification layers in air (Figure 6). As well known, oxygen could cause the oxidation of organic materials in the active layer, and the increase of the hole concentration inside the active layer may result in the carrier concentration to be out of balance [63]. In air atmosphere, the devices modified with ZnO, SnO_2 and SnO_2/ZnO showed decay efficiency to 68%, 72% and 83% of the initial device after six months, respectively. The device with SnO_2/ZnO exhibited better efficiency stability compared to the devices with SnO_2 and ZnO in air due to the denser film formed by the double cathode modification layer, which can efficiently prevent the water and oxygen molecules from entering into the device, so that effectively reduce the influence of water and oxygen in the air.

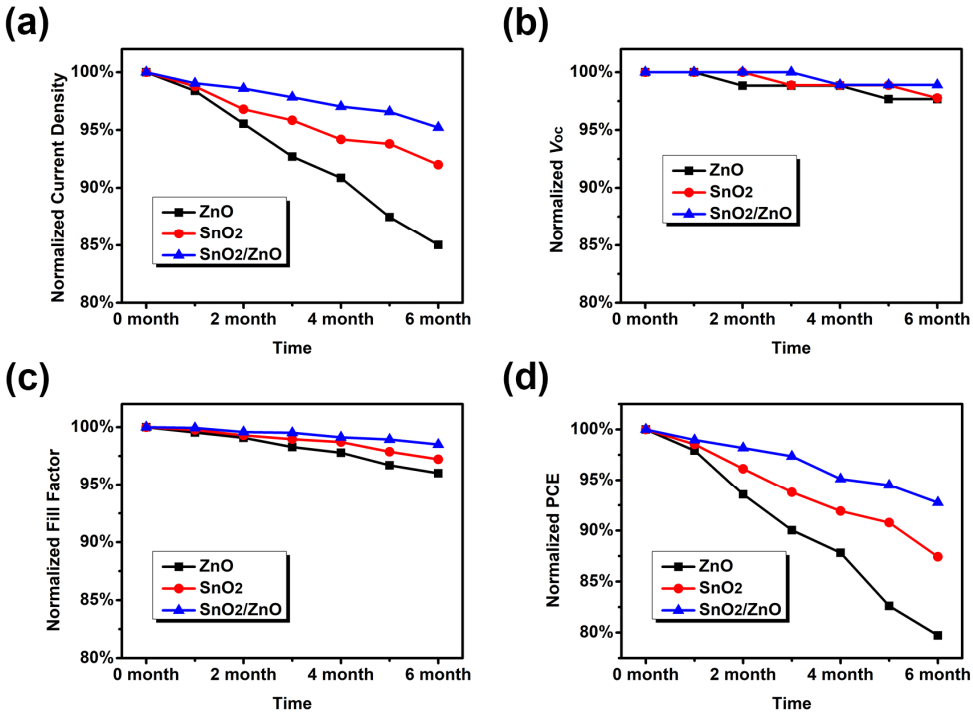

Figure 5. The normalized photovoltaic performance curves of devices in purity nitrogen atmosphere: (**a**) for J_{SC}; (**b**) for V_{OC}; (**c**) for FF; (**d**) for PCE.

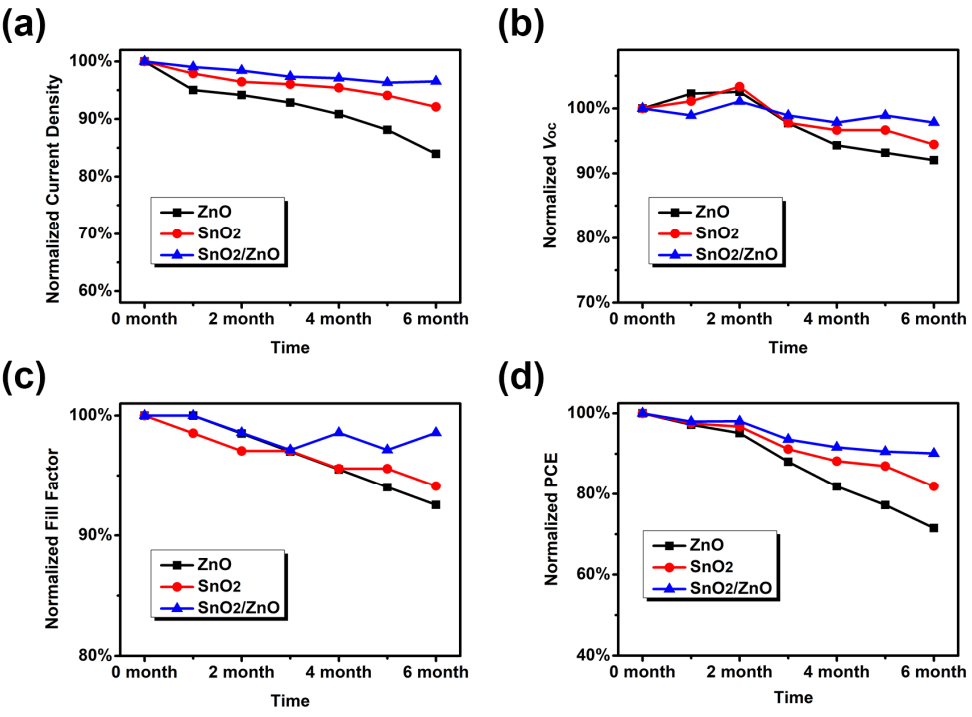

Figure 6. The normalized photovoltaic performance curves of devices in air: (**a**) for J_{SC}; (**b**) for V_{OC}; (**c**) for FF; (**d**) for PCE.

It is worth noting that the performance degradation of ZnO modified device is the most severe in both nitrogen atmosphere and air, and it is mainly due to the decline of J_{SC}. This is most likely due to the strong absorption of UV by ZnO, which leads to the photodegradation of IT-4F, and the addition of SnO_2 layer can effectively alleviate this problem [64]. In conclusion, the adoption of SnO_2/ZnO films as cathode modification layer

is proved to be an effective strategy to enhance the stability of OSCs, which could reduce the rate of dark-degradation both in nitrogen atmosphere and air condition.

4. Conclusions

In summary, we have prepared high-efficiency and high stability inversion OSCs based on PM7:IT-4F system by introducing the SnO_2/ZnO film as a double cathode modification layer. Herein, we revealed the mechanism of improving the device performance and stability via SnO_2/ZnO cathode modification layer. The advantages of both single ZnO and SnO_2 films are reflected in SnO_2/ZnO double cathode modified layer. Cover the ZnO on the SnO_2 film efficiently passivate the surface defects of SnO_2, and fabricate a SnO_2 film before ZnO film is more conducive to electron transport and block holes. Compared to the single cathode modification layer, the SnO_2/ZnO buffer layer enhances the PCE of OSCs obviously to 12.91% with a FF of 70%, a J_{SC} of 20.04 mA/cm^2 and a V_{OC} of 0.92 V. The results obtained from charge transport and extraction study via TPV/TPC, Photo-CELIV measurements and dependence of V_{OC}/J_{SC} on light intensity imply the reducing energy barrier between the electrode and active layer and the reducing trap near the interface layer, which result in suppressed charge recombination, efficient charge transfer and collection near the active layer/(SnO_2/ZnO) interface. Furthermore, the denser SnO_2/ZnO modification layer, on one hand, prevents the downward infiltration of the active material into electrode, and on the other hand, efficiently reduces the immigration of water and oxygen into the interface between modification layer and active layer, which significantly slowed down the dark-degradation in both nitrogen and air atmosphere with a degradation rate of 7% in nitrogen, and 17% in air. Our work not only provides the method to fabricate OSCs with high efficiency and stability through double cathode modification layer, but more importantly elaborates the underlying mechanisms associated with improving the device efficiency and stability via cathode modification, which would provide new inspiration in the relevant studies.

Supplementary Materials: The following supporting information can be downloaded at: https://www.mdpi.com/article/10.3390/en15207643/s1, Figure S1: Atomic force microscopy (AFM) images of the ZnO (a,d), SnO_2 (b,e) and SnO_2/ZnO (c,f) films. In addition, the root-mean-square (RMS) roughness of the ZnO, SnO_2 and SnO_2/ZnO films are 2.95 nm, 1.76 nm and 1.94 nm, respectively; Figure S2: Ultraviolet photoelectron spectrometry (UPS) spectra of the ZnO, SnO_2 and SnO_2/ZnO films; Table S1: The secondary electron cutoff and work function derived from UPS spectra.

Author Contributions: Conceptualization, T.L. and T.D.; methodology, T.D.; validation, T.L.; formal analysis, T.D.; investigation, T.L.; resources, T.L.; data curation, T.L.; writing—original draft preparation, T.D.; writing—review and editing, T.L.; visualization, T.D.; supervision, T.L.; project administration, T.L.; funding acquisition, T.L. All authors have read and agreed to the published version of the manuscript.

Funding: Supported by the Research Foundation for Youth Scholars of Beijing Technology and Business University, grant number QNJJ2022-42.

Data Availability Statement: Not applicable.

Acknowledgments: The authors are very grateful for the support by the Research Foundation for Youth Scholars of Beijing Technology and Business University.

Conflicts of Interest: The authors declare no conflict of interest.

References

1. Cheng, P.; Yan, C.; Wu, Y.; Wang, Y.; Qin, M.; An, Q.; Cao, J.; Huo, L.; Zhang, F.; Ding, L.; et al. Alloy Acceptor: Superior Alternative to PCBM toward Efficient and Stable Organic Solar Cells. *Adv. Mater.* **2016**, *28*, 8021–8028. [CrossRef]
2. Cui, Y.; Xu, Y.; Yao, H.; Bi, P.; Hong, L.; Zhang, J.; Zu, Y.; Zhang, T.; Qin, J.; Ren, J.; et al. Single-Junction Organic Photovoltaic Cell with 19% Efficiency. *Adv. Mater.* **2021**, *33*, 2102420. [CrossRef] [PubMed]
3. Qin, F.; Sun, L.; Chen, H.; Liu, Y.; Lu, X.; Wang, W.; Liu, T.; Dong, X.; Jiang, P.; Jiang, Y.; et al. 54 cm^2 Large-Area Flexible Organic Solar Modules with Efficiency Above 13%. *Adv. Mater.* **2021**, *33*, 2103017. [CrossRef] [PubMed]

4. Liu, Y.; Liu, G.; Xie, R.; Wang, Z.; Zhong, W.; Li, Y.; Huang, F.; Cao, Y. A Rational Design and Synthesis of Cross-Conjugated Small Molecule Acceptors Approaching High-Performance Fullerene-Free Polymer Solar Cells. *Chem. Mater.* **2018**, *30*, 4331–4342. [CrossRef]
5. Zhu, C.; Meng, L.; Zhang, J.; Qin, S.; Lai, W.; Qiu, B.; Yuan, J.; Wan, Y.; Huang, W.; Li, Y. A Quinoxaline-Based D-A Copolymer Donor Achieving 17.62% Efficiency of Organic Solar Cells. *Adv. Mater.* **2021**, *33*, 2100474. [CrossRef] [PubMed]
6. Yuan, J.; Zhang, Y.; Zhou, L.; Zhang, G.; Yip, H.; Lau, T.; Lu, X.; Zhu, C.; Peng, H.; Johnson, P.A.; et al. Single-Junction Organic Solar Cell with over 15% Efficiency Using Fused-Ring Acceptor with Electron-Deficient Core. *Joule* **2019**, *3*, 1140–1151. [CrossRef]
7. Liu, Q.; Jiang, Y.; Jin, K.; Qin, J.; Xu, J.; Li, W.; Xiong, J.; Liu, J.; Xiao, Z.; Sun, K.; et al. 18% Efficiency organic solar cells. *Sci. Bull.* **2020**, *65*, 272–275. [CrossRef]
8. Zhan, L.; Li, S.; Xia, X.; Li, Y.; Lu, X.; Zuo, L.; Shi, M.; Chen, H. Layer-by-Layer Processed Ternary Organic Photovoltaics with Efficiency over 18%. *Adv. Mater.* **2021**, *33*, 2007231. [CrossRef] [PubMed]
9. Hong, L.; Yao, H.; Cui, Y.; Bi, P.; Zhang, T.; Cheng, Y.; Zu, Y.; Qin, J.; Yu, R.; Ge, Z.; et al. 18.5% Efficiency Organic Solar Cells with a Hybrid Planar/Bulk Heterojunction. *Adv. Mater.* **2021**, *33*, 2103091. [CrossRef]
10. Wang, J.; Zheng, Z.; Zu, Y.; Wang, Y.; Liu, X.; Zhang, S.; Zhang, M.; Hou, J. A Tandem Organic Photovoltaic Cell with 19.6% Efficiency Enabled by Light Distribution Control. *Adv. Mater.* **2021**, *33*, 2102787. [CrossRef]
11. Zhang, M.; Zhu, L.; Hao, T.; Zhou, G.; Qiu, C.; Zhao, Z.; Hartmann, N.; Xiao, B.; Zou, Y.; Feng, W.; et al. High-Efficiency Organic Photovoltaics using Eutectic Acceptor Fibrils to Achieve Current Amplification. *Adv. Mater.* **2021**, *33*, 2007177. [CrossRef] [PubMed]
12. Lou, S.J.; Szarko, J.M.; Xu, T.; Yu, L.; Marks, T.J.; Chen, L.X. Effects of additives on the morphology of solution phase aggregates formed by active layer components of high-efficiency organic solar cells. *J. Am. Chem. Soc.* **2011**, *133*, 20661–20663. [CrossRef] [PubMed]
13. Dai, T.; Li, X.; Zhang, Y.; Xu, D.; Geng, A.; Zhao, J.; Chen, X. Performance improvement of polymer solar cells with binary additives induced morphology optimization and interface modification simultaneously. *Sol. Energy* **2020**, *201*, 330–338. [CrossRef]
14. Cai, C.; Yao, J.; Chen, L.; Yuan, Z.; Zhang, Z.; Hu, Y.; Zhao, X.; Zhang, Y.; Chen, Y.; Li, Y. Silicon Naphthalocyanine Tetraimides: Cathode Interlayer Materials for Highly Efficient Organic Solar Cells. *Angew. Chem. Int. Ed.* **2021**, *60*, 19053–19057. [CrossRef] [PubMed]
15. Meng, H.; Liao, C.; Deng, M.; Xu, X.; Yu, L.; Peng, Q. 18.77% Efficiency Organic Solar Cells Promoted by Aqueous Solution Processed Cobalt(II) Acetate Hole Transporting Layer. *Angew. Chem. Int. Ed.* **2021**, *60*, 22554–22561. [CrossRef] [PubMed]
16. Liu, L.; Chen, S.; Qu, Y.; Gao, X.; Han, L.; Lin, Z.; Yang, L.; Wang, W.; Zheng, N.; Liang, Y.; et al. Nanographene-Osmapentalyne Complexes as a Cathode Interlayer in Organic Solar Cells Enhance Efficiency over 18%. *Adv. Mater.* **2021**, *33*, 2101279. [CrossRef]
17. Yu, Z.; Xia, Y.; Du, D.; Ouyang, J. PEDOT:PSS Films with Metallic Conductivity through a Treatment with Common Organic Solutions of Organic Salts and Their Application as a Transparent Electrode of Polymer Solar Cells. *ACS Appl. Mater. Interfaces* **2016**, *8*, 11629–11638. [CrossRef]
18. Girotto, C.; Voroshazi, E.; Cheyns, D.; Heremans, P.; Rand, B.P. Solution-processed MoO_3 thin films as a hole-injection layer for organic solar cells. *ACS Appl. Mater. Interfaces* **2011**, *3*, 3244–3247. [CrossRef]
19. Aqoma, H.; Park, S.; Park, H.; Hadmojo, W.T.; Oh, S.; Nho, S.; Kim, D.; Seo, J.; Park, S.; Ryu, D.Y.; et al. 11% Organic Photovoltaic Devices Based on PTB7-Th: PC71BM Photoactive Layers and Irradiation-Assisted ZnO Electron Transport Layers. *Adv. Sci.* **2018**, *5*, 1700858. [CrossRef]
20. Wen, X.; Fang, S.; Xu, Y.; Zheng, N.; Liu, L.; Xie, Z.; Würthner, F. Enhanced Electron Transportation by Dye Doping in Very Low-Temperature (<130 °C)-Processed Sol-Gel ZnO toward Flexible Organic Solar Cells. *ACS Appl. Mater. Interfaces* **2019**, *11*, 34151–34157. [CrossRef]
21. You, J.; Chen, C.; Dou, L.; Murase, S.; Duan, H.; Hawks, S.A.; Xu, T.; Son, H.; Yu, L.; Li, G.; et al. Metal oxide nanoparticles as an electron-transport layer in high-performance and stable inverted polymer solar cells. *Adv. Mater.* **2012**, *24*, 5267–5272. [CrossRef] [PubMed]
22. Brabec, C.J.; Shaheen, S.E.; Winder, C.; Sariciftci, N.S. Effect of LiF/metal electrodes on the performance of plastic solar cells. *Appl. Phys. Lett.* **2002**, *80*, 1288–1290. [CrossRef]
23. Yu, S.; Yang, W.; Li, L.; Zhang, W. Improved Chemical Stability of ITO Transparent Anodes with a SnO_2 Buffer Layer for Organic Solar Cells. *Sol. Energy Mater. Sol. Cells* **2016**, *144*, 652–656. [CrossRef]
24. Lee, E.; Heo, S.; Han, Y.; Moon, D. An organic-inorganic hybrid interlayer for improved electron extraction in inverted polymer solar cells. *J. Mater. Chem. C* **2016**, *4*, 2463–2469. [CrossRef]
25. He, R.; Yu, L.; Cai, P.; Peng, F.; Xu, J.; Ying, L.; Chen, J.; Yang, W.; Cao, Y. Narrow-Band-Gap Conjugated Polymers Based on 2,7-Dioctyl-Substituted Dibenzo[*a*,*c*]phenazine Derivatives for Polymer Solar Cells. *Macromolecules* **2014**, *47*, 2921–2928. [CrossRef]
26. Xiong, S.; Hu, L.; Hu, L.; Sun, L.; Qin, F.; Liu, X.; Fahlman, M.; Zhou, Y. 12.5% Flexible Nonfullerene Solar Cells by Passivating the Chemical Interaction Between the Active Layer and Polymer Interfacial Layer. *Adv. Mater.* **2019**, *31*, 1806616. [CrossRef]
27. Pan, F.; Sun, C.; Li, Y.; Tang, D.; Zou, Y.; Li, X.; Bai, S.; Wei, X.; Lv, M.; Chen, X.; et al. Solution-Processable n-Doped Graphene-Containing Cathode Interfacial Materials for High-Performance Organic Solar Cells. *Energy Environ. Sci.* **2019**, *12*, 3400–3411. [CrossRef]
28. Zhang, Z.; Qi, B.; Jin, Z.; Chi, D.; Qi, Z.; Li, Y.; Wang, J. Perylene Diimides: A Thickness-Insensitive Cathode Interlayer for High Performance Polymer Solar Cells. *Energy Environ. Sci.* **2014**, *7*, 1966–1973. [CrossRef]

29. Zhou, P.; Yang, Y.; Chen, X.; Zhang, Z.; Li, Y. Design of a Thiophene-fused Benzotriazole Unit as an Electron Acceptor to Build D-A Copolymers for Polymer Solar Cells. *J. Mater. Chem. C* **2017**, *5*, 2951–2957. [CrossRef]
30. Jiang, T.; Yang, J.; Tao, Y.; Fan, C.; Xue, L.; Zhang, Z.; Li, H.; Li, Y.; Huang, W. Random Terpolymer with a Cost-effective Monomer and Comparable Efficiency to PTB7-Th for Bulk-heterojunction Polymer Solar Cells. *Polym. Chem.* **2016**, *7*, 926–932. [CrossRef]
31. Uddin, A.; Upama, M.B.; Yi, H.; Duan, L. Encapsulation of Organic and Perovskite Solar Cells: A Review. *Coatings* **2019**, *9*, 65. [CrossRef]
32. Burlingame, Q.; Ball, M.; Loo, Y. It's time to focus on organic solar cell stability. *Nat. Energy* **2020**, *5*, 947–949. [CrossRef]
33. Duan, L.; Uddin, A. Progress in Stability of Organic Solar Cells. *Adv. Sci.* **2020**, *7*, 1903259. [CrossRef]
34. Hains, A.W.; Liu, J.; Martinson, A.B.F.; Irwin, M.D.; Marks, T.J. Anode Interfacial Tuning via Electron-Blocking/Hole-Transport Layers and Indium Tin Oxide Surface Treatment in Bulk-Heterojunction Organic Photovoltaic Cells. *Adv. Funct. Mater.* **2010**, *20*, 595–606. [CrossRef]
35. Son, H.; Kim, S.; Kim, D. Critical Impact of Hole Transporting Layers and Back Electrode on the Stability of Flexible Organic Photovoltaic Module. *Adv. Energy Mater.* **2017**, *7*, 1601289. [CrossRef]
36. Shaikh, S.F.; Kwon, H.; Yang, W.; Hwang, H.; Lee, H.; Lee, E.; Ma, S.; Moon, J. La_2O_3 interface modification of mesoporous TiO_2 nanostructures enabling highly efficient perovskite solar cells. *J. Mater. Chem. A* **2016**, *4*, 15478–15485. [CrossRef]
37. Shaikh, S.F.; Kwon, H.; Yang, W.; Mane, R.S.; Moon, J. Performance enhancement of mesoporous TiO_2-based perovskite solar cells by ZnS ultrathin-interfacial modification layer. *J. Alloys Compd.* **2018**, *738*, 405–414. [CrossRef]
38. Khan, U.; Iqbal, T.; Khan, M.; Wu, R. SnO_2/ZnO as double electron transport layer for halide perovskite solar cells. *Sol. Energy* **2021**, *223*, 346–350. [CrossRef]
39. Fan, Q.; Zhu, Q.; Xu, Z.; Su, W.; Chen, J.; Wu, J.; Guo, X.; Ma, W.; Zhang, M.; Li, Y. Chlorine substituted 2D-conjugated polymer for high-performance polymer solar cells with 13.1% efficiency via toluene processing. *Nano Energy* **2018**, *48*, 413–420. [CrossRef]
40. Pan, M.; Lau, T.; Tang, Y.; Wu, Y.; Liu, T.; Li, K.; Chen, M.; Lu, X.; Ma, W.; Zhan, C. 16.7%-efficiency ternary blended organic photovoltaic cells with PCBM as the acceptor additive to increase the open-circuit voltage and phase purity. *J. Mater. Chem. A* **2019**, *7*, 20713–20722. [CrossRef]
41. Zhang, Z.; Liu, X.; Yu, J.; Wang, H.; Zhang, M.; Yang, L.; Geng, R.; Cao, J.; Du, F.; Liu, F.; et al. Enhancing phase separation with a conformation-locked nonfullerene acceptor for over 14.4% efficiency solar cells. *J. Mater. Chem. C* **2019**, *7*, 13279–13286. [CrossRef]
42. Wang, C.; Jiang, B.; Lu, J.; Cheng, M.; Jeng, R.; Lu, Y.; Chen, C.; Wong, K. A Near-Infrared Absorption Small Molecule Acceptor for High-Performance Semitransparent and Colorful Binary and Ternary Organic Photovoltaics. *ChemSusChem* **2020**, *13*, 903–913. [CrossRef] [PubMed]
43. Cheng, J.; Zhang, L.; Jiang, H.; Yuan, D.; Wang, Q.; Cao, Y.; Chen, J. Investigation of halogen-free solvents towards high-performance additive-free non-fullerene organic solar cells. *Org. Electron.* **2020**, *85*, 105871. [CrossRef]
44. Dai, T.; Li, X.; Zhang, Y.; Zhou, X.; Zhu, Y.; Zhou, J.; Xu, D.; Lin, T. Electric-Induced Degradation of Cathode Interface Layer in PM7:IT-4F Polymer Solar Cells. *Sol. RRL* **2021**, *5*, 2100151. [CrossRef]
45. Zhou, X.; Dai, T.; Li, X.; Yan, Y.; Xiong, W.; Lin, T.; Zhou, J.; Xu, D.; Zhu, Y.; Zhao, J.; et al. Improved Charge Transport and Reduced Carrier Recombination of Nonfullerene Organic Solar Cells with the Binary Solvent. *ACS Appl. Energy Mater.* **2021**, *4*, 8175–8182. [CrossRef]
46. Tran, V.; Eom, S.; Yoon, S.; Kim, S.; Lee, S. Enhancing device performance of inverted organic solar cells with SnO_2/Cs_2CO_3 as dual electron transport layers. *Org. Electron.* **2019**, *68*, 85–95. [CrossRef]
47. Ai, Y.; Liu, W.; Shou, C.; Yan, J.; Li, N.; Yang, Z.; Song, W.; Yan, B.; Sheng, J.; Ye, J. SnO_2 surface defects tuned by $(NH_4)_2S$ for high-efficiency perovskite solar cells. *Sol. Energy* **2019**, *194*, 541–547. [CrossRef]
48. Xiong, Y.; Lin, Y.; Wang, X.; Zhao, Y.; Tian, J. Defect engineering on SnO_2 nanomaterials for enhanced gas sensing performances. *Adv. Powder Mater.* **2022**, *1*, 100033. [CrossRef]
49. An, Q.; Ma, X.; Gao, J.; Zhang, F. Solvent additive-free ternary polymer solar cells with 16.27% efficiency. *Sci. Bull.* **2019**, *64*, 504–506. [CrossRef]
50. Chen, J.; Zhang, L.; Jiang, X.; Gao, K.; Liu, F.; Gong, X.; Chen, J.; Cao, Y. Using o-Chlorobenzaldehyde as a Fast Removable Solvent Additive during Spin-Coating PTB7-Based Active Layers: High Efficiency Thick-Film Polymer Solar Cells. *Adv. Energy Mater.* **2017**, *7*, 1601344. [CrossRef]
51. Xiao, J.; Chen, Z.; Zhang, G.; Li, Q.; Yin, Q.; Jiang, X.; Huang, F.; Xu, Y.; Yip, H.; Cao, Y. Efficient device engineering for inverted non-fullerene organic solar cells with low energy loss. *J. Mater. Chem. C* **2018**, *6*, 4457–4463. [CrossRef]
52. Blom, P.W.M.; Mihailetchi, V.D.; Koster, L.J.A.; Markov, D.E. Device Physics of Polymer:Fullerene Bulk Heterojunction Solar Cells. *Adv. Mater.* **2007**, *19*, 1551–1566. [CrossRef]
53. Li, Z.; Gao, F.; Greenham, N.C.; McNeill, C.R. Comparison of the Operation of Polymer/Fullerene, Polymer/Polymer, and Polymer/Nanocrystal Solar Cells: A Transient Photocurrent and Photovoltage Study. *Adv. Funct. Mater.* **2011**, *21*, 1419–1431. [CrossRef]
54. Chatri, A.R.; Torabi, S.; Corre, V.M.L.; Koster, L.J.A. Impact of Electrodes on Recombination in Bulk Heterojunction Organic Solar Cells. *ACS Appl. Mater. Interfaces* **2018**, *10*, 12013–12020. [CrossRef]
55. Soci, C.; Moses, D.; Xu, Q.; Heeger, A.J. Charge-carrier Relaxation Dynamics in Highly Ordered Poly(p-phenylene vinylene): Effects of Carrier Bimolecular Recombination and Trapping. *Phys. Rev. B* **2005**, *72*, 245204. [CrossRef]

56. Stephen, M.; Genevičius, K.; Juška, G.; Arlauskas, K.; Hiorns, R.C. Charge transport and its characterization using photo-CELIV in bulk heterojunction solar cells. *Polym. Int.* **2017**, *66*, 13–25. [CrossRef]
57. Cowan, S.R.; Roy, A.; Heeger, A.J. Recombination in polymer-fullerene bulk heterojunction solar cells. *Phys. Rev. B* **2010**, *82*, 245207. [CrossRef]
58. Huang, S.; Tang, Y.; Yu, A.; Wang, Y.; Shen, S.; Kang, B.; Silva, S.R.P.; Lu, G. Solution-processed SnO_2 Nanoparticle Interfacial Layers for Efficient Electron Transport in ZnO-based Polymer Solar Cells. *Org. Electron.* **2018**, *62*, 373–381. [CrossRef]
59. Yin, Z.; Zheng, Q.; Chen, S.; Cai, D. Interface Control of Semiconducting Metal Oxide Layers for Efficient and Stable Inverted Polymer Solar Cells with Open-Circuit Voltages over 1.0 Volt. *ACS Appl. Mater. Interfaces* **2013**, *5*, 9015–9025. [CrossRef] [PubMed]
60. Sandberg, O.J.; Nyman, M. Charge extraction by a linearly increasing voltage of photo-generated carriers: The influence of two mobile carrier types, bimolecular recombination, and series resistance. *Org. Electron.* **2019**, *64*, 97–103. [CrossRef]
61. Neukom, M.; Züfle, S.; Jenatsch, S.; Ruhstaller, B. Opto-electronic characterization of third-generation solar cells. *Sci. Technol. Adv. Mater.* **2018**, *19*, 291–316. [CrossRef] [PubMed]
62. Song, K.; Singh, R.; Lee, J.; Sin, D.; Lee, H.; Cho, K. Propeller-shaped small molecule acceptors containing a 9,9′-spirobifluorene core with imide-linked perylene diimides for non-fullerene organic solar cells. *J. Mater. Chem. C* **2016**, *4*, 10610–10615. [CrossRef]
63. Dkhil, S.B.; Pfannmöller, M.; Schröder, R.R.; Alkarsifi, R.; Gaceur, M.; Köntges, W.; Heidari, H.; Bals, S.; Margeat, O.; Ackermann, J.; et al. Interplay of Interfacial Layers and Blend Composition To Reduce Thermal Degradation of Polymer Solar Cells at High Temperature. *ACS Appl. Mater. Interfaces* **2018**, *10*, 3874–3884. [CrossRef] [PubMed]
64. Jiang, Y.; Sun, L.; Jiang, F.; Xie, C.; Hu, L.; Dong, X.; Qin, F.; Liu, T.; Hu, L.; Jiang, X.; et al. Photocatalytic effect of ZnO on the stability of nonfullerene acceptors and its mitigation by SnO_2 for nonfullerene organic solar cells. *Mater. Horiz.* **2019**, *6*, 1438–1443. [CrossRef]